Applied Catalysis B: Environmental 180 (2016) 740–750

Contents lists available at ScienceDirect

Applied Catalysis B: Environmental

journal homepage: www.elsevier.com/locate/apcatb

Adsorption and photocatalysis of 2-ethyl-1-hexanol over graphene oxide–TiO_2 hybrids post-treated under various thermal conditions

Ho-Hwan Chun[a], Wan-Kuen Jo[b,*]

[a] Department of Naval Architecture and Ocean Engineering, Pusan National University, Busan 609-735, Republic of Korea
[b] Department of Environmental Engineering, Kyungpook National University, Daegu, 702–701, Republic of Korea

ARTICLE INFO

Article history:
Received 21 January 2015
Received in revised form 15 June 2015
Accepted 14 July 2015
Available online 21 July 2015

Keywords:
Post-treatment temperature
Photocatalyst characteristic
Adsorption property
Mineralization efficiency
Gaseous intermediate

ABSTRACT

High temperature (>300 °C) post-treatment of two-dimensional graphene oxide-coupled titania (GO–TiO_2) hybrids may enhance their photocatalytic performances. This concept has not yet been fully assessed. In the present study, we explored the applicability of GO–TiO_2 hybrids synthesized using a chemical mixing method, followed by post-treatment under various thermal conditions (200–500 °C), for the degradation of low-concentration gas-phase 2-ethyl-1-hexanol (2E1H) in continuous-flow mode under visible-light illumination. The morphological and optical characteristics of the synthesized photocatalysts were investigated by field-emission transmission electron microscopy, thermal gravimetric analysis, X-ray diffraction technique, X-ray photoelectron spectroscopy, ultraviolet-visible spectroscopy, and N_2 adsorption–desorption analysis. The GO–TiO_2 hybrid post-treated at 400 °C exhibited longer breakthrough and saturation times and a higher capacity for 2E1H adsorption than did GO–TiO_2 post-treated at 200 °C. The photocatalytic 2E1H degradation efficiencies of the post-treated GO–TiO_2 hybrids were superior to those of the untreated GO–TiO_2 hybrid and neat TiO_2 samples. Moreover, the photocatalytic activities of the GOkTiO_2 hybrids increased as the post-treatment temperature increased from 200 to 400 °C, and decreased as the temperature was further increased to 500 °C, indicating that the treatment temperature can be increased up to at least 400 °C without significant reduction of the photocatalytic performance. The photocatalytic activity of the GO–TiO_2 hybrid post-treated at 400 °C depended strongly on three process parameters: relative humidity, initial contaminant concentration, and catalyst mass. There was no appreciable loss of photocatalytic efficiency for the GO–TiO_2 hybrid post-treated at 400 °C after five cycles. The average 2E1H mineralization efficiency was 55.1%, while the average photocatalytic efficiency was 99.3%. Two gaseous organic compounds, i.e., 3-heptanone and 2-ethyl hexanal, and carbon monoxide were identified as the primary partially oxidized intermediates. The average carbon monoxide concentration (0.49 ppm) was well below the permissible 8-h exposure level (25 ppm).

1. Introduction

Indoor air pollution is a serious environmental issue because it has been closely linked with various adverse health effects on building occupants, such as sick building syndrome, carcinogenic effects, blood-related disorders, and damage to the nervous system and liver [1,2]. Volatile organic compounds (VOCs) are one of the most important pollutant groups that influence indoor air quality (IAQ) in non-industrial buildings; they originate from a range of indoor sources such as domestic cleaning agents, furnishings, floor coverings, and wallpaper, as well as infiltration of polluted outdoor air [3,4]. In particular, 2-ethyl-1-hexanol (2E1H), a VOC, has been detected in the indoor air in many countries, including European countries, Singapore, and Japan at high concentrations (up to nearly 0.1 ppm) over a long-term period [5,6]. Moreover, this pollutant can cause bad odors, pseudo-asthmatic symptoms, and eye and throat irritation [7]. In many buildings, 2E1H primarily originates from poly(vinyl chloride) building materials, water-damaged floor constructions, and cement-based flooring materials through the reactions of esters (e.g., 2-ethylhexyl-acrylate) with water under alkaline conditions [8,9]. Therefore, the development of methods for mitigating 2E1H is necessary to minimize indoor exposure of building inhabitants.

Photocatalytic techniques using semiconductor titania (TiO_2) nanoparticles have been extensively used for the purification of a great deal of environmental pollutants, including VOCs [10,11]. However, real-world utilizations of TiO_2 for pollutant treatments

* Corresponding author. Fax: +82 53 950 6579/+82 53 950 6584.
E-mail address: wkjo@knu.ac.kr (W.-K. Jo).

http://dx.doi.org/10.1016/j.apcatb.2015.07.021
0926-3373/

are hampered by low quantum availability, low adsorption capacity, and broad band gaps [12,13]. The use of combinations of TiO_2 with carbonaceous materials has been suggested to tackle these drawbacks, because of the synergistic electron transfer interactions at the interface between the two components, high adsorptivity of carbon materials, and modified band gaps [14,15]. In particular, a single-atom-thick graphene oxide (GO) sheet, which can be synthesized by simply exfoliating graphite oxide, has emerged as a promising two-dimensional carbon substrate that can be coupled with TiO_2 nanoparticles to enhance the photocatalytic activity [16,17]. In TiO_2 photocatalysts combined with two-dimensional GO (GO–TiO_2) hybrids, the oxygenated functional groups on the GO sheets facilitate the binding of TiO_2 and GO [18], and GOs can serve as electron sinks under ultraviolet (UV) illumination or electron donors under visible light illumination for retardation of electron-hole recombination [16,19]. Additionally, the surface areas of GO–TiO_2 hybrids (e.g., 80 $m^2\,g^{-1}$) are higher than that of uncoupled TiO_2 (e.g., 57 $m^2\,g^{-1}$) [16]. GOs may also expand the light-absorbance range to include visible light, because GOs can behave as impurities, forming Ti—O—C bonds and providing various mid-band-gap states [19].

Previous research [16,17,19,20] showed that both GO–TiO_2 and reduced GO–TiO_2 (RGO–TiO_2) hybrids had photocatalytic activities superior to that of pure TiO_2 under visible light or UV illumination for the decomposition of dyes or chromium ions in aqueous media, or aromatic hydrocarbons and methanol in air. Specifically, Roso et al. [20] reported enhanced photocatalytic efficiencies of UV-activated RGO–TiO_2-based photocatalysts on nanostructured membranes compared with that of pure TiO_2 for the decomposition of gaseous methanol. Nguyen-Phan et al. [19] observed that the photocatalytic performances of UV- or visible light-driven GO–TiO_2 hybrids synthesized via a colloidal mixing method were superior to that of neat TiO_2 in the decomposition of aqueous-phase methylene blue, and that their photocatalytic performances improved as the GO content increased. Jiang et al. [16] found that the decomposition efficiency of a GO–TiO_2 hybrid, prepared using a liquid-phase deposition method, under UV irradiation for methyl orange was approximately 95%, whereas that of neat TiO_2 was <40%. However, previous research did not involve thermal post-treatment processes, or only used low-temperature post-treatment processes (100–300 °C), for the synthesis of GO–TiO_2 hybrids. It is notable that the GO in GO–TiO_2 hybrids can be thermally stabilized by the interactions of TiO_2 with oxygenated functional groups on the two-dimensional GO sheets [16]. This suggests that increasing the post-treatment temperature for GO–TiO_2 hybrids (>300 °C) could enhance their photocatalytic performances without significant loss of their hybrid characteristics. Thus far, this concept has not been fully assessed.

In this study, GO–TiO_2 hybrids were synthesized using a chemical blending method, followed by post-treatment under various thermal conditions (200–500 °C). The adsorption and photocatalytic characteristics of the prepared GO–TiO_2 hybrids, with respect to airborne 2E1H, were evaluated without and with visible-light illumination. Low-level concentrations (sub-ppm) of the target compound were utilized to approximate IAQ levels. Unlike those of commercially available P25 TiO_2, the mineralization efficiencies of neither the GO–TiO_2 hybrids nor the intermediates formed during the heterogeneous photocatalysis of gas-phase pollutants have been well documented. In this study, therefore, we also attempted to address this issue. In addition, the photocatalytic activities of a GO–TiO_2 hybrid without heat treatment and neat TiO_2 samples prepared using the same process, but without the addition of GO, were examined for comparison.

2. Methodology

2.1. Photocatalysts

The GO–TiO_2 hybrids were prepared by blending GO with a Ti precursor, with or without a thermal post-treatment process. Oxidized graphite was first synthesized using modified version of previously reported methods [21,22]. In brief, 10 g of cleaned graphite powder (<20 μm, Sigma–Aldrich) was slowly mixed with 230 mL of cold concentrated H_2SO_4 (98%, Duksan) in an ice bath, to keep the temperature below 10 °C, with stirring. 30 g of $KMnO_4$ (99%, Sigma–Aldrich) was slowly added to this solution, which was then heated to 35 °C in a water bath and held at that temperature for 120 min, after which 460 mL of deionized water was added. After 40 min, 150 mL of deionized water and 30 mL of H_2O_2 (30%, Sigma–Aldrich) were added. The formed suspension was centrifuged to obtain a precipitate. The precipitate was cleaned with HCl (37%, Sigma–Aldrich), acetone (HPLC, Sigma–Aldrich), and distilled water. The cleaned product was conditioned at 65 °C for 20 h to provide oxidized graphite.

For synthesis of the GO–TiO_2 hybrids, 0.075 g of oxidized graphite powder was mixed with 100 mL of deionized water. The mixture was ultrasonicated for 120 min to obtain a GO dispersion (0.75 $g\,L^{-1}$). The GO dispersion was mixed with 250 mL of deionized water, and then 0.028 mol of ammonium hexafluorotitanate (IV) ($(NH_4)_2TiF_6$, Sigma–Aldrich) and 0.084 mol of hydrogen borate (H_3BO_3, Sigma–Aldrich) were added with vigorous stirring, then heated to 60 °C in a water bath, and held at that temperature for 2 h. The mixture was filtered, cleaned with deionized water, and dried at 100 °C for 2 h. The weight ratio of GO–TiO_2 was calculated to be 0.033. Thermal post-treatments of the products were performed at 200, 300, 400, and 500 °C for 2 h to obtain GO–TiO_2 hybrids, denoted by GO–TiO_2-200, GO–TiO_2-300, GO–TiO_2-400, and GO–TiO_2-500, respectively; the non-heat treated GO–TiO_2 hybrid is denoted by GO–TiO_2-nt. Neat TiO_2 samples were also prepared using the same process, but without the addition of GO, followed by thermal post-treatments at 200, 300, 400, and 500 °C, denoted by TiO_2-200, TiO_2-300, TiO_2-400, and TiO_2-500, respectively. The characteristics of the prepared GO–TiO_2 hybrids and a neat TiO_2 (TiO_2-300) were examined using field-emission transmission electron microscopy (FE-TEM; FEI Titan G2 chemiSTEM Cs Probe), thermal gravimetric analysis (TGA; TA Instruments SDT Q600 TG), X-ray diffraction (XRD; Rigaku D/max-2500), X-ray photoelectron spectroscopy (PHI Quantera SXM), UV-visible spectroscopy (Varian CARY 5G diffuse reflectance spectrometer), and N_2 adsorption–desorption isotherm analysis (Micromeritics ASAP 2020).

2.2. Adsorption and photocatalysis of 2E1H

Five different experiments were designed to investigate the adsorption characteristics and photocatalysis of gas-phase 2E1H over the prepared photocatalysts. A Pyrex reactor (internal diameter 3.7 cm and volume 206 cm^3), the inside wall of which was coated with a specified photocatalyst, was utilized for the experiments. A cylindrical fluorescent lamp (Youngwha Lamp F8T5DL, 400–720 nm) was placed inside another Pyrex tube (outer diameter 1.9 cm). The outside face of the tube reactor was covered with an aluminum sheet to prevent light transmission from laboratory light sources. Humidified air was directed to flow through the empty space between the two Pyrex tubes. The relative humidity was regulated by mixing pure dried air with a specified portion of water-saturated air, which was produced by flowing pure dried air through water bottles. The air-stream flow rate (1–4 $L\,min^{-1}$) was monitored using a mass flow meter (Bios International Co., Defender 510-H). Samples of 2E1H of known concentrations were prepared in a heated mixing vessel by controlling the volume

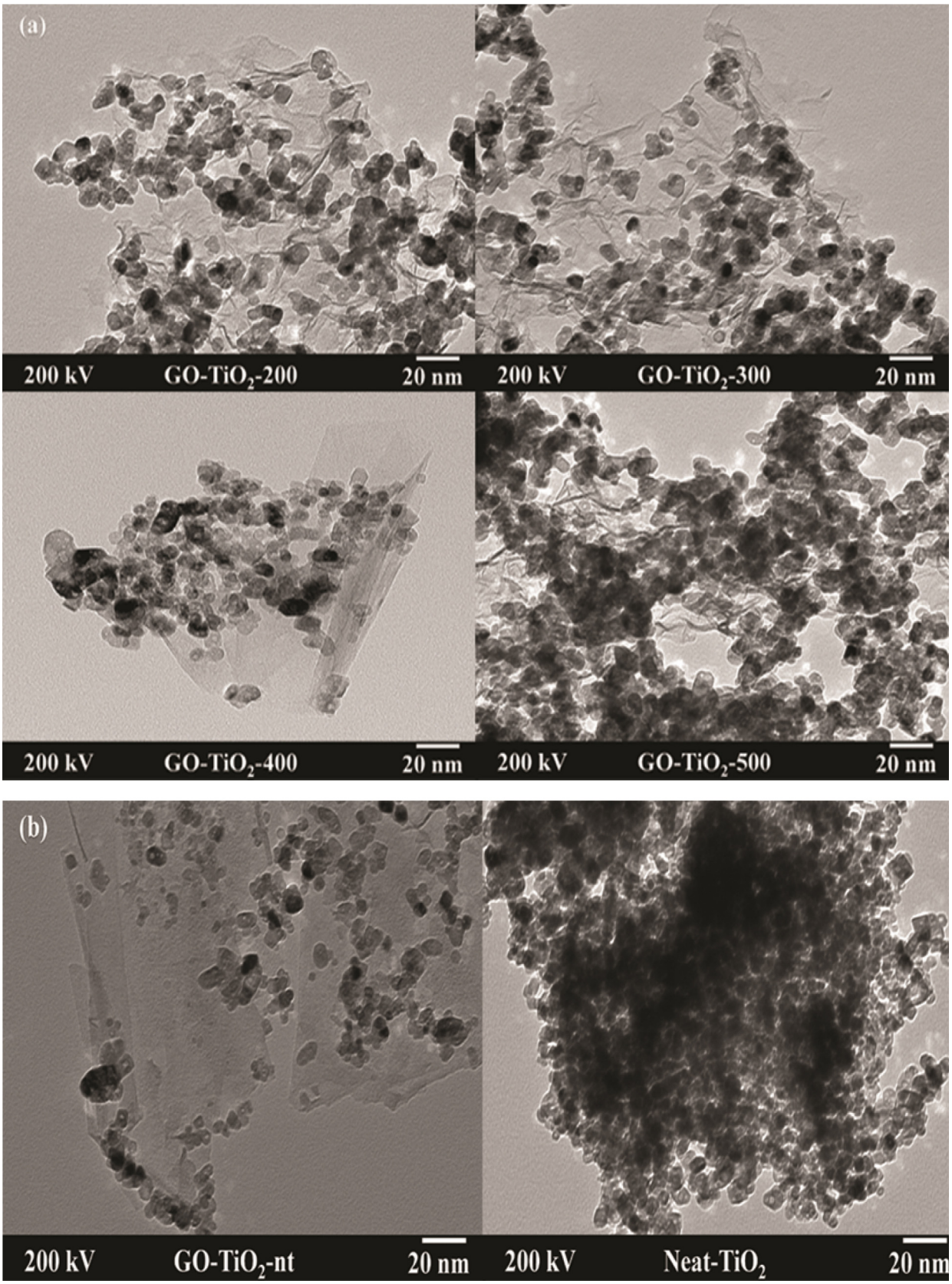

Fig. 1. Field-emission transmission electron microscopy images of (a) heat-treated GO–TiO_2 hybrids (GO–TiO_2-200, GO–TiO_2-300, GO–TiO_2-400, and GO–TiO_2-500) and (b) GO–TiO_2-nt and neat TiO_2 (TiO_2-300).

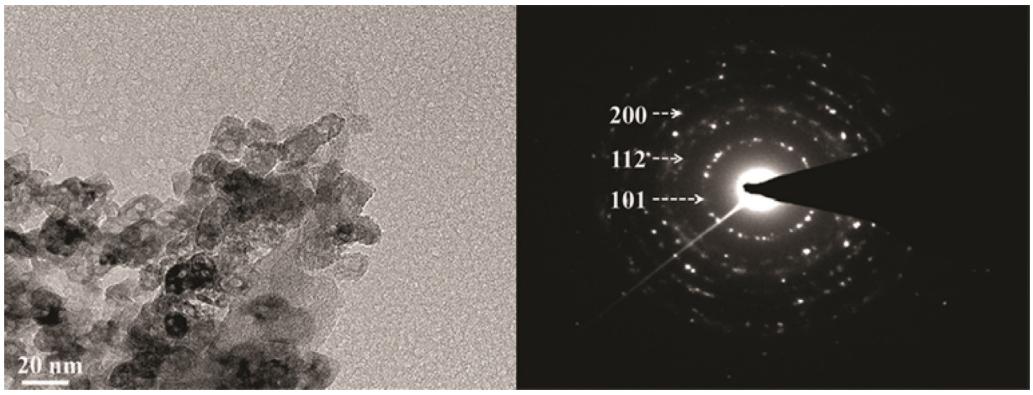

Fig. 2. Magnified FE-TEM image and selected area electron diffraction pattern of GO–TiO_2-400.

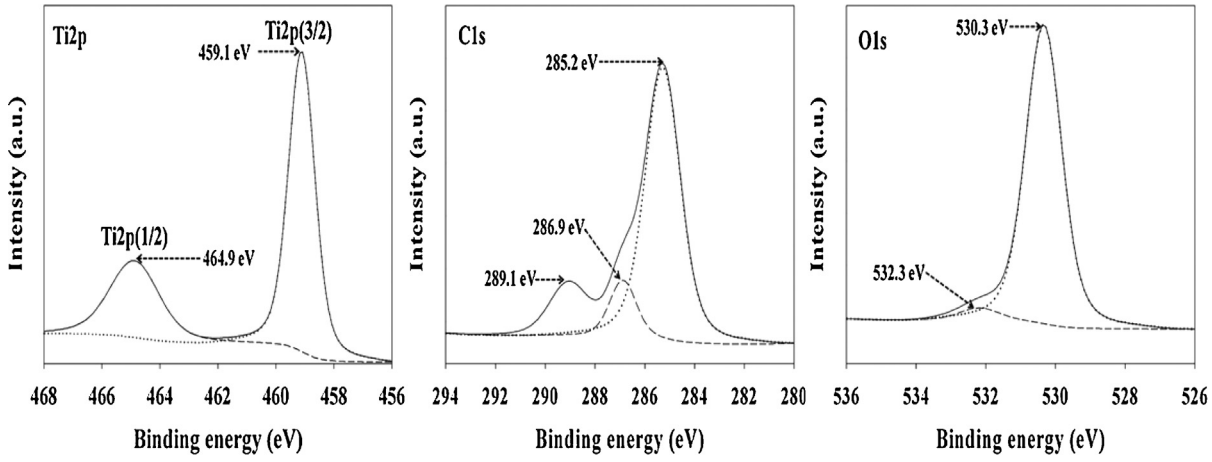

Fig. 3. Ti2p, C1s, and O1s X-ray photoelectron spectra for GO–TiO_2-400.

mixing ratios of a standard chemical, infused using a syringe pump (KDScientific Legato 100), to the influent humidified air. For the first experiment (Experiment I), the inner face of the larger Pyrex tube was coated with 0.3 mg cm^{-2} of either GO–TiO_2-200 or GO–TiO_2-400. The flow rate of the air directed to the reactor was 1 L min^{-1}, and the input concentration was fixed at 0.1 ppm. The second experiment (Experiment II) was performed using six different photocatalysts (GO–TiO_2-200, GO–TiO_2-300, GO–TiO_2-400, GO–TiO_2-500, GO–TiO_2-nt, and TiO_2-300) at the same input concentration (0.1 ppm) as in the first experiment. However, for this experiment, the reactor was coated with a lower amount of photocatalyst (0.1 mg cm^{-2}) and a higher air flow rate (3 L min^{-1}) was used, to reduce the time required to reach adsorption saturation of 2E1H on the photocatalyst surface. The third experiment (Experiment III) was performed to assess the effects of process parameters, using a reactor coated with GO–TiO_2-400 and a flow rate of 4 L min^{-1}. The three major parameters tested in this experiment were relative humidity (20–80%), initial contaminant concentration (0.1–2.0 ppm), and catalyst mass (0.05–0.2 mg cm^{-2}). When assessing one parameter, the other parameters were adjusted to the following values: relative humidity, 50%; initial concentration, 0.1 ppm; catalyst mass, 0.1 mg cm^{-2}. The fourth experiment (Experiment IV) was performed to examine the formation of intermediates and the mineralization efficiency, and the photocatalytic degradation efficiency, using a reactor coated with 0.1 mg cm^{-2} of GO–TiO_2-400. For this experiment, a high 2E1H input concentration (0.8 ppm) and a low flow rate (1 L min^{-1}) were used to achieve better quantitative analyses of the intermediates, carbon monoxide (CO), and carbon dioxide (CO_2) with concentration levels well above their detection limits. In the last experiment (Experiment V), five cycles of 2E1H decomposition were performed to assess the stability of GO–TiO_2-400 under the following conditions: flow rate, 4 L min^{-1}; relative humidity, 50%; initial concentration, 0.1 ppm; catalyst mass, 0.1 mg cm^{-2}.

A preliminary control photolysis test was performed using an uncoated reactor under lamp illumination. Prior to performing the adsorption and photocatalysis tests, the coated photocatalytic system was pre-purified for 10 h by supplying humidified air through the system under light irradiation. When no contamination with any organic vapors was observed in the photocatalytic unit, a standard gas-containing air stream was allowed to flow into the reactor in the absence of light illumination. After adsorption–desorption equilibrium of 2E1H between the air stream and photocatalyst was established, the light source was activated. Organic vapor samples were taken periodically at the input and output streams of the reactor, using an empty Tedlar bag, and then the samples were transferred into an adsorbent (Tenax GC)-containing trap. The organic vapors were determined using a gas chromatography (GC)/mass spectrometry (MS) system (PerkinElmer Clarus SQ 8) coupled to a thermal desorption system (PerkinElmer ATD 350). 2E1H and major gas-phase intermediates were identified from their retention times, the mass spectra of standard substrates, and the Wiley 275 software library, with a fit greater than 90%. Their quantities were determined using calibration curves established by analyzing standard chemicals at five different concentrations each. The measurement quality of vaporous organic species was controlled by analyzing laboratory blanks and spiked Tenax-GC traps, and by determining the method detection limit for 2E1H

(0.0005 ppm). The organic species adsorbed on the photocatalyst surface were identified using a solid–liquid extraction procedure, followed by GC/MS analyses.

The CO and CO_2 concentrations in the input and output air streams of the reactor were concurrently monitored using an on-line GC with a CH_4 converter (Synspec B.V. Alpha 12) and a packed column (3.2 mm × 1.8 m, Agilent HayeSep R). For a sample measurement, air flowing at 50 mL min^{-1} was drawn from the photocatalytic unit into the GC system for 1 min. The temperatures of the GC oven and CH_4 converter were 40 and 320 °C, respectively. The analysis time for one sample with a carrier gas (nitrogen, N_2) flow of 4 mL min^{-1} was 7 min. Calibration of CO and CO_2 was performed using standard gases at five different concentrations each. The detection limit of the instrument was 0.1 ppm for both gases.

3. Results and discussion

3.1. Characteristics of GO–TiO_2 hybrids and neat TiO_2

The prepared photocatalysts were characterized using various optical and spectroscopic methods. The morphological properties of the prepared photocatalysts were investigated using FE-TEM spectra. The FE-TEM analysis (Fig. 1a and b) shows that the GO–TiO_2 hybrids displayed lower aggregation of nanoparticles than did a neat TiO_2 (TiO_2-300). Nguyen-Phan et al. [19] also observed that GO–TiO_2 hybrids synthesized using a colloidal mixing process, without thermal post-treatment, and using P25 TiO_2 as a Ti source, showed low particle agglomeration compared with P25 TiO_2 nanoparticles. The low aggregation of GO–TiO_2 hybrids probably results from the high dispersion of TiO_2 nanoparticles on the surfaces of two-dimensional GO nano-sheets, and the high aggregation of neat TiO_2 powder is ascribed to the strong tendency of TiO_2 nanoparticles to self-aggregate [16]. Additionally, the selected area electron diffraction pattern of GO–TiO_2-400 displayed anatase crystal phases corresponding to 101 ($2\theta = 25.28°$), 112 ($2\theta = 38.58°$), and 200 ($2\theta = 48.05°$) planes, demonstrating that the dark spots in the image are anatase TiO_2 (Fig. 2).

The Ti2p, C1s, and O1s XPS images of GO–TiO_2-400 were obtained to provide insights into its surface properties (Fig. 3). The Ti2p XP spectrum had two distinctive peaks, with central positions at 464.9 and 459.1 eV, which are associated with Ti2p(1/2) and Ti2p(3/2) of Ti^{4+}, respectively. Meanwhile, no peaks, with central positions at 465.8 and 460.2 eV, which are associated with Ti—C band in the sample [16], were observed, suggesting the absence of Ti—C band in the GO–TiO_2-400. Deconvolution of the C1s region gave three distinct peaks, with central positions at 289.1, 286.9, and 285.2 eV, which correspond to O=C—O, C—O, and C—C, respectively. In addition, the O1s XP spectrum had two peaks, with central positions at 532.3 and 530.3 eV, which are associated with C=O and Ti—O, respectively.

Fig. 4 shows the TG-differential thermal analysis curves of GO–TiO_2-nt, GO–TiO_2-400, GO–TiO_2-500, GO, and neat TiO_2 (TiO_2-300). Pure GO powder showed distinct mass losses in three stages over the temperature range 30–800 °C. The first-stage loss (19.2%), observed between 30 and 146 °C, is attributed to the desorption and evaporation of water molecules adsorbed on the sample surface [23]. The second-stage loss (27.5%), observed in the range 146–210 °C, is ascribed to the release of carbon oxide compounds and other oxygenated functional groups attached to GO [16,23]. The final-stage loss (20.3%), observed in the range 300–700 °C, is probably associated with initial dehydroxylation of the catalyst surface and combustion of carbon substrates [18,24]. In contrast to pure GO, GO–TiO_2-nt did not show a distinct three-stage weight loss. Instead, the GO–TiO_2-nt curve showed a gentle slope, with a weight loss of 22.1% in the temperature range 30–600 °C. The curve for

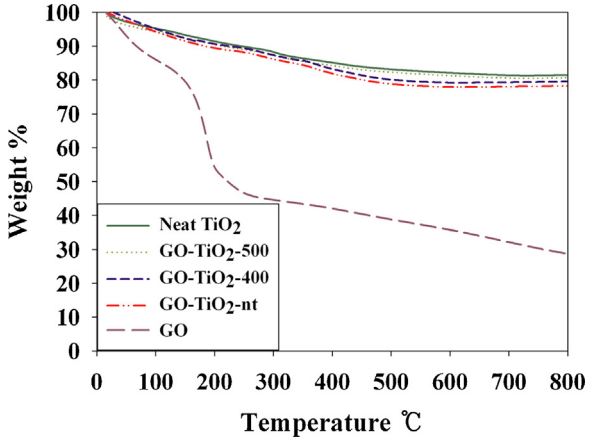

Fig. 4. Thermal gravimetric analysis and differential thermal analysis curves of GO–TiO_2-nt, GO–TiO_2-400, GO–TiO_2-500, GO, and neat TiO_2 (TiO_2-300).

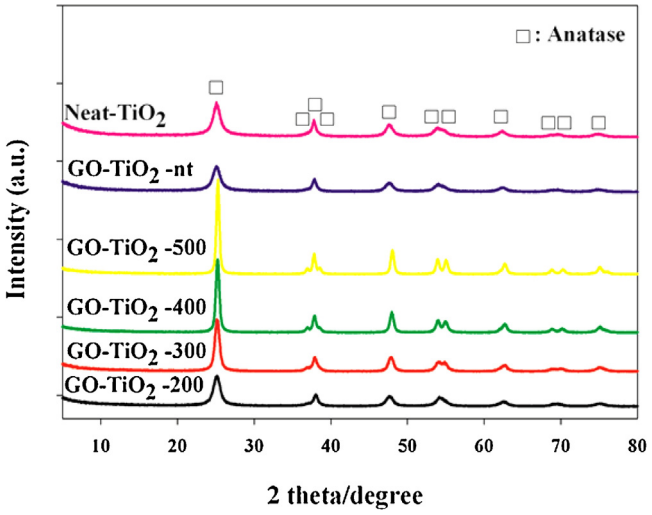

Fig. 5. X-ray diffraction patterns of (a) GO–TiO_2-200, (b) GO–TiO_2-300, (c) GO–TiO_2-400, (d) GO–TiO_2-500, (e) GO–TiO_2-nt, and (f) neat TiO_2 (TiO_2-300).

neat TiO_2 displayed a similar gentle slope, with a weight loss of 18.5% in the range 30–675 °C. Lambert et al. [18] also reported that non-thermally treated GO–TiO_2 hybrids, which were prepared via hydrolysis of TiF_4 followed by chemical and thermal reduction, had a slow weight loss relative to that of neat GO. A comparison of the TG-differential thermal curves of GO and GO–TiO_2-nt confirms that GO can be thermally stabilized by embedded TiO_2 particles, probably as a result of bonding between oxygen functional groups on the GO surface and TiO_2 nanoparticles. The GO–TiO_2-400 and GO–TiO_2-500 TGA curves displayed gentle slopes, with weight losses of 20.8% and 19.5%, respectively, in the temperature range 30–600 °C. The lower weight loss for GO–TiO_2-500 is partly ascribed to greater loss of GO from GO–TiO_2-500 during the calcination process compared with that from GO–TiO_2-400, because of more extensive combustion of the carbon constituents at higher calcination temperatures [25]. The TGA results suggest that the GO content of GO–TiO_2-400 is higher than that of GO–TiO_2-500.

The XRD patterns of the prepared photocatalysts are shown in Fig. 5. The XRD spectra of the GO–TiO_2 hybrids and neat TiO_2 (TiO_2-300) were similar, displaying exclusively anatase crystal bands with a dominant band at $2\theta = 25.2°$; they did not display rutile phase peaks. These results suggest that the GO–TiO_2 hybrids retain the nanocrystalline structure of TiO_2. The anatase peak intensity of the non-thermally treated GO–TiO_2 hybrid (GO–TiO_2-nt) was

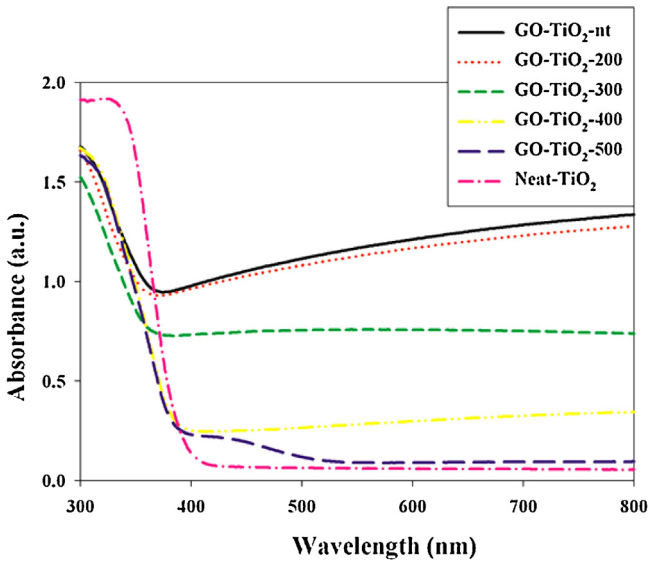

Fig. 6. Ultraviolet-visible absorption spectra of (a) GO–TiO_2-200, (b) GO–TiO_2-300, (c) GO–TiO_2-400, (d) GO–TiO_2-500, (e) GO–TiO_2-nt, and (f) neat TiO_2 (TiO_2-300).

lower than that for neat TiO_2 post-treated at 300 °C. Moreover, the intensity and number of anatase peaks increased as the thermal-treatment temperature of the GO–TiO_2 hybrids increased, because of the enhanced crystallinity of TiO_2 at high temperatures. The crystallite sizes, which are closely associated with crystallinity [26], followed the order GO–TiO_2-nt (10.6 nm) < GO–TiO_2-200 (11.0 nm) < GO–TiO_2-300 (14.0 nm) < GO–TiO_2-400 (18.0 nm) < GO–TiO_2-500 (21.8 nm). However, no GO-associated peak, which is typically deep and broad and appears at 2θ=24.5° [27], was observed in the XRD images of the GO–TiO_2 hybrids. These findings are attributed to low GO contents in the hybrids, which would be less than the measurement limit of the analytical instrument.

Fig. 6 shows the optical properties of the synthesized photocatalysts, based on UV-visible absorbance spectra. Neat TiO_2 exhibited an absorbance edge at ~400 nm, but a red shift into the visible region occurred for the GO–TiO_2 hybrids. This is attributed to band gap narrowing caused by the influence of GOs in the optical properties [19]. In addition, GO–TiO_2-nt exhibited the strongest absorption intensity and longest absorption edge, and both the visible-light absorption intensity and absorption edge decreased with increasing post-treatment temperature. The light absorption edges of GO–TiO_2-nt, GO–TiO_2-200, GO–TiO_2-300, GO–TiO_2-400, and GO–TiO_2-500 were at 465, 445, 420, 410, and 405 nm, respectively. The decreasing visible-light absorption of the GO–TiO_2 hybrids with increasing calcination temperature is ascribed to greater loss of GO from the hybrids; this was previously indicated by the TGA results (Fig. 4). Nevertheless, the results suggest that the synthesized GO–TiO_2 hybrids can function properly under visible-light illumination.

N_2 adsorption–desorption analysis and the Brunauer–Emmett–Teller (BET) method were applied to determine the physical properties of the prepared photocatalysts. As illustrated in Table 1, the surface areas and porosities of the GO–TiO_2 hybrids were higher than those of neat TiO_2; this is ascribed to the high adsorption capacity of two-dimensional GO sheets. Previous researchers [19] reported that the surface areas and pore volumes of GO–TiO_2 were higher than those of pure P25 TiO_2. Moreover, GO–TiO_2 hybrids post-treated at higher temperatures showed higher surface areas and pore volumes. The specific surface area and pore volume of GO–TiO_2-500 were 113.8 $m^2\,g^{-1}$ and 0.47 $cm^3\,g^{-1}$, respectively, whereas the values for GO–TiO_2-nt were 68.5 $m^2\,g^{-1}$ and 0.23 $cm^3\,g^{-1}$, respectively.

Table 1
Textural properties of thermally post-treated and non-treated GO–TiO_2 hybrids, and neat TiO_2

Photocatalyst	Specific surface area ($m^2\,g^{-1}$)	Total pore volume ($cm^3\,g^{-1}$)
GO–TiO_2-200	84.0	0.32
GO–TiO_2-300	95.7	0.39
GO–TiO_2-400	100.3	0.41
GO–TiO_2-500	113.8	0.47
GO–TiO_2-nt	68.5	0.23
Neat TiO_2 (TiO_2-300)	38.7	0.14

3.2. Adsorption and photocatalytic properties

In Experiment I, the adsorption and photocatalytic properties of gas-phase 2E1H over two GO–TiO_2 hybrids treated at different temperatures (GO–TiO_2-200 and GO–TiO_2-400) were examined at a relative humidity of 50%, photocatalyst coating amount of 0.3 mg cm^{-2}, flow rate of 1 L min^{-1}, and 2E1H input concentration of 0.1 ppm. The adsorption breakthrough profiles of 2E1H obtained using the two photocatalysts without light illumination are shown in Fig. 7. GO–TiO_2-400 exhibited longer breakthrough and saturation times for 2E1H adsorption than did GO–TiO_2-200 (Table 2). Specifically, the breakthrough and saturation times for GO–TiO_2-400 were 49–51 h and 91–93 h, respectively, while the values for GO–TiO_2-200 were 7–8 h and 80–82 h, respectively.

In addition, the adsorption capacities of GO–TiO_2-200 and GO–TiO_2-400 were determined using the input and output concentrations observed during the adsorption process, based on the following equations:

$$A_c = \frac{M_c}{M_p} \quad (1)$$

$$Mc = \sum m_i (2)$$

$$m_i = \int_0^t (C_{in} - C_{out,i}(t))Q_a dt \quad (3)$$

where A_C is the adsorption capacity of 2E1H on the photocatalyst (mg g^{-1}), M_p is the mass of the photocatalyst (g), M_c is the total mass of 2E1H adsorbed on the photocatalyst (mg), m_i is the mass of 2E1H adsorbed on the photocatalyst (mg) during the i^{th} adsorption period, C_{in} is the input concentration of 2E1H (0.53 mg m^{-3}, which was converted from 0.1 ppm), $C_{out,i}(t)$ is the outlet concentration of 2E1H (mg m^{-3}) determined downstream of the reactor during the i^{th} adsorption period, and Q_a is the air flow rate ($m^3\,min^{-1}$). Table 2 shows that the adsorption capacity of GO–TiO_2-400 (29.1 mg g^{-1}) was nearly three times higher than that of GO–TiO_2-200 (10.2 mg g^{-1}). The higher 2E1H adsorption capacity of GO–TiO_2-400, and longer breakthrough and saturation times are attributed to a higher surface area and total pore volume relative to those of GO–TiO_2-200 (Table 1). Fig. 7 illustrates that the 2E1H input-to-output concentration ratios obtained with both GO–TiO_2-200 and GO–TiO_2-400 decreased sharply within 10 min of light illumination and then approached a quasi-steady state. These results are ascribed to gradual photocatalytic degradation of 2E1H molecules adsorbed on the surfaces of the GO–TiO_2 hybrids in the presence of light. Consistent with the adsorption capacity, the photocatalytic activity of GO–TiO_2-400 was greater than that of GO–TiO_2-200. Overall, the results indicate that the post-treatment temperature is a crucial parameter and influences both the adsorption properties and photocatalytic performances of GO–TiO_2 hybrids.

Table 2
Breakthrough times, saturation periods, and adsorption capacities of 2E1H over GO–TiO_2-200 and GO–TiO_2-400 each with a coating amount of 0.3 mg cm^{-2}

Hybrid	Breakthrough time, h	Saturation period, h	Adsorption capacity (mg g^{-1})
GO–TiO_2-200	7–8	80–82	10.2
GO–TiO_2-400	49–51	91–93	29.1

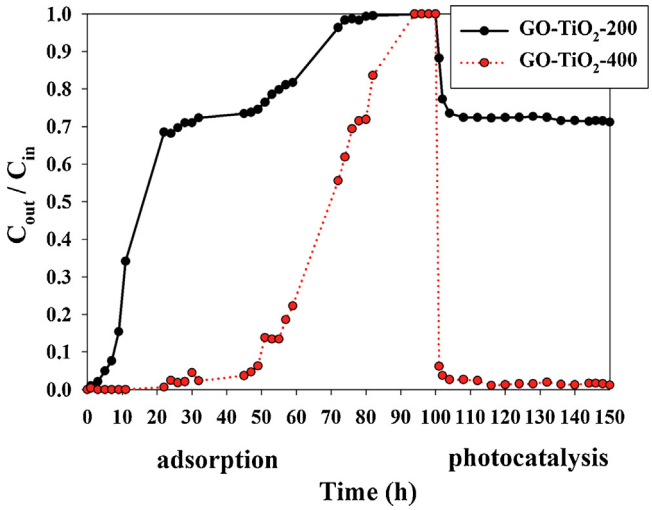

Fig. 7. Time-series for 2E1H adsorption and photocatalysis over GO–TiO_2-200 and GO–TiO_2-400, without and with visible-light irradiation; each reactor coated using same amount of photocatalyst (0.3 mg cm^{-2}).

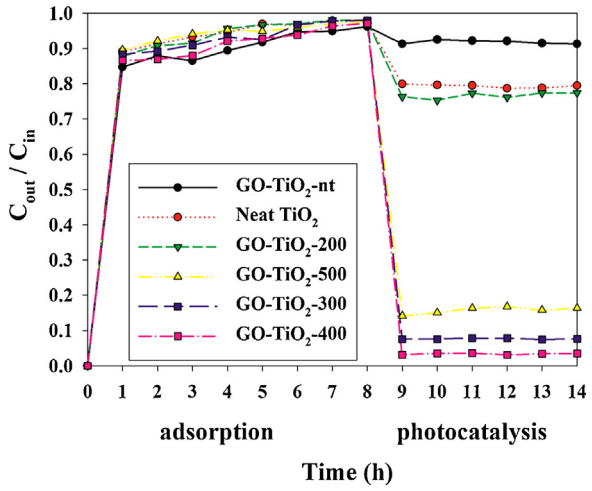

Fig. 8. Time-series ratios of input to output concentrations of 2E1H over GO–TiO_2-200, GO–TiO_2-300, GO–TiO_2-400, GO–TiO_2-500, GO–TiO_2-nt, and neat TiO_2 (TiO_2-300) without and with visible-light irradiation; each sample coated using same amount of photocatalyst (0.1 mg cm^{-2}).

In Experiment II, the adsorption and photocatalytic properties of gas-phase 2E1H over five GO–TiO_2 hybrids, either untreated or post-treated at different temperatures (GO–TiO_2-nt, GO–TiO_2-200, GO–TiO_2-300, GO–TiO_2-400, and GO–TiO_2-500), and neat TiO_2 post-treated at 300 °C (TiO_2-300) were examined at a relative humidity of 50%, photocatalyst coating amount of 0.1 mg cm^{-2}, flow rate of 3 L min^{-1}, and 2E1H input concentration of 0.1 ppm. Fig. 8 shows the 2E1H input-to-output concentration ratios over the GO–TiO_2 hybrids treated at various temperatures, GO–TiO_2-nt, and neat TiO_2 in the presence and absence of light illumination. The adsorption breakthrough (<1 h) and saturation (~8 h) times shown in Fig. 8 are much shorter than those shown in Fig. 7 (data obtained from Experiment I). As previously mentioned, this difference is ascribed to the much lower photocatalyst amounts and higher air flow rates in Experiment II. In addition, the control photolysis experiment showed that there was no degradation of the target compound, indicating that the decreases in the 2E1H input-to-output concentration ratios over the photocatalysts in the presence of light were primarily caused by photocatalytic degradation.

As shown in Fig. 8, the photocatalytic activities of the thermally post-treated GO–TiO_2 hybrids were higher than those of the untreated GO–TiO_2 hybrid and TiO_2-300 under visible-light illumination. The 2E1H input-to-output concentration ratios ranged from 0.03 to 0.77 for the thermally post-treated GO–TiO_2 hybrids, whereas the average values for the untreated GO–TiO_2 hybrid and TiO_2-300 were 0.90 and 0.79, respectively. The enhanced photocatalytic activities of the thermally post-treated GO–TiO_2 hybrids are attributed to unique roles of GO in the photocatalytic reactions: high GO adsorption and efficient charge transfer [14,15,25,28]. As shown in Table 1, the thermally post-treated GO–TiO_2 hybrids had higher surface areas and pore volumes, probably because of the two-dimensional honeycomb-like network structure of GO sheets. In carbonaceous nanomaterial-coupled TiO_2 hybrids, GO and other carbon materials can act as excellent supports for pollutant adsorption; the adsorbed pollutants migrate to TiO_2 nanoparticles by diffusion, thereby improving the photocatalytic performances of the hybrids [15]. In addition, GOs in GO–TiO_2 hybrids under visible light illumination can serve as sensitizers (electron donors) of TiO_2 that transfers electrons from the conduction band of the GO–TiO_2, reducing the recombination of charge carriers and enabling GO–TiO_2 hybrids to function effectively under visible-light irradiation [19,25,28]. Moreover, the photocatalytic efficiencies of the thermally treated samples were higher than that of GO–TiO_2-nt, although their visible light absorption intensity was weaker (Fig. 6). Notably, the surface areas (Table 1) and the crystallinities (Fig. 5) of the thermally treated samples were greater than those of GO–TiO_2-nt. Therefore, one possible explanation for the higher photocatalytic activities of the thermally treated samples is that the effects of surface area and crystallinity outweigh the effect of visible-light absorption on the photocatalytic activities of GO–TiO_2 hybrids. Taken together, the results show that thermally post-treated GO–TiO_2 hybrids can be used to treat IAQ-level 2E1H under visible-light illumination. Additionally, the photocatalytic efficiency of GO–TiO_2-nt was lower than that of TiO_2-300. This low activity is probably a result of the higher crystallinity of neat TiO_2 (Fig. 4), because neat TiO_2 was thermally treated at 300 °C, whereas GO–TiO_2-nt was not thermally treated. Meanwhile, the photocatalytic efficiencies of neat TiO_2 samples did not significantly vary with increasing treatment temperature (Fig. 9).

Fig. 8 shows that the photocatalytic efficiencies of the GO–TiO_2 hybrids increased with increasing post-treatment temperature from 200 to 400 °C, and decreased as the temperature was further increased to 500 °C. The average 2E1H input-to-output concentration ratios over the GO–TiO_2-200, GO–TiO_2-300, GO–TiO_2-400, and GOkTiO$_2$-500 hybrids were 0.78, 0.09, 0.03, and 0.15, respectively, indicating that there is an optimal post-treatment temperature. The lowest ratio was observed for GO–TiO_2-400; this indicates that GO–TiO_2-400 had the highest photocatalytic activity, suggesting that the thermal treatment temperature can be increased up to at least 400 °C to enhance the photocatalytic activities of GO–TiO_2 hybrids. The increase in the photocatalytic activity with increasing temperature up to 400 °C is attributed to enhancement of the TiO_2 crystallinities (Fig. 5), BET surface areas, and

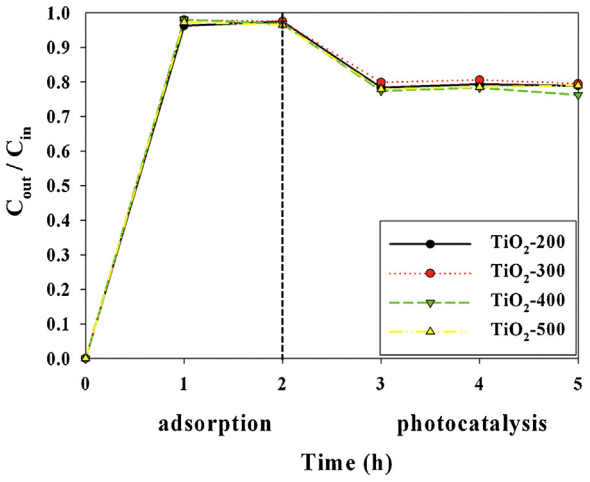

Fig. 9. Time-series ratios of input to output concentrations of 2E1H over TiO_2-200, TiO_2-300, TiO_2-400, and TiO_2-500 under visible-light irradiation; each sample coated using same amount of photocatalyst (0.1 mg cm^{-2}).

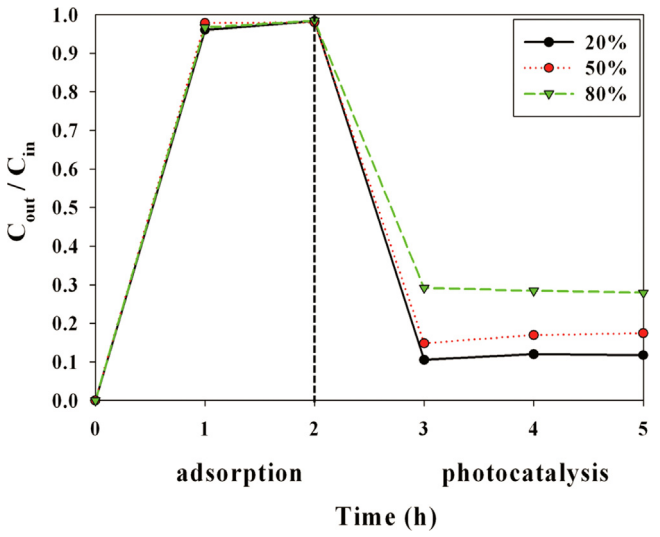

Fig. 10. Time-series ratios of input to output concentrations of 2E1H over GO–TiO_2-400 under visible-light irradiation, according to relative humidity (20%, 50%, and 80%); coated amount of photocatalyst, 0.1 mg cm^{-2}.

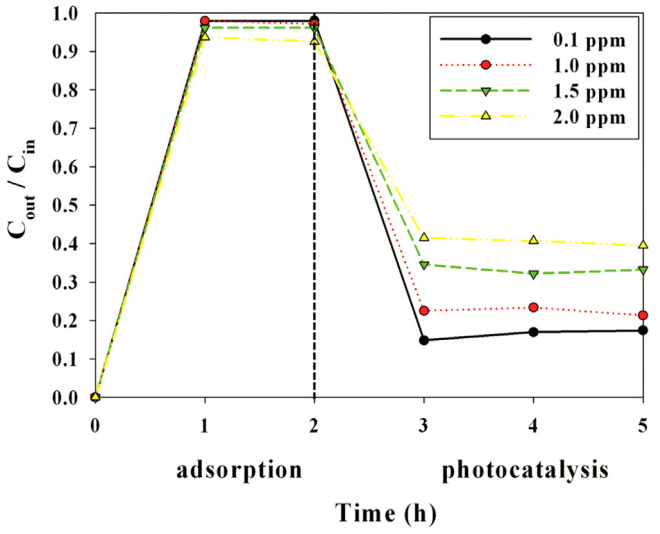

Fig. 11. Time-series ratios of input to output concentrations of 2E1H over GO–TiO_2-400 under visible-light irradiation, according to initial concentration (0.1, 1.0, 1.5, and 2.0 ppm); coated amount of photocatalyst, 0.1 mg cm^{-2}.

pore volumes of the GO–TiO_2 hybrids (Table 1) as a result of the high-temperature conditions. Meanwhile, the visible-light absorption for GO–TiO_2-400 was weaker than those of GO–TiO_2-200 and GO–TiO_2-300. These results suggest that the effects of surface and structural properties exceeded the effects of light absorption on the photocatalytic efficiencies of the GO–TiO_2 hybrids. Moreover, the photocatalytic efficiency for GO–TiO_2-400 was higher than that for GO–TiO_2-500. For GO–TiO_2-400, the thermal degradation of the GO components was lower, as indicated by the TGA results (Fig. 4), and the visible-light absorption was stronger (Fig. 6), compared with those of GO–TiO_2-500; but its crystallinities (Fig. 5) and surface areas (Table 1) were lower. In this case, therefore, the effects of the amount of GO and the light absorption might outweigh the effects of crystallinity and surface area on the photocatalytic efficiencies of the GO–TiO_2 hybrids. Consequently, the effect of calcination temperature on the photocatalytic activities of the GO–TiO_2 hybrids does not appear to depend consistently on the process parameters, but instead appears to depend on a variety of process parameters in a complex way. Jiang et al. [16] also found that the photocatalytic performances of GO–TiO_2 hybrids varied with the calcination temperature. However, they reported that the photocatalytic efficiencies of GO–TiO_2 hybrids in the aqueous-phase decomposition of methyl orange decreased as the calcination temperature increased from 200 to 250 °C. The difference between the results of the present and previous studies is attributed to several operating parameters such as the substrates, light energies and intensities, media, amounts of photocatalyst tested, and ratios of GO–TiO_2.

In Experiment III, the effects of three major process parameters (relative humidity, initial contaminant concentration, and catalyst mass) on the photocatalytic efficiency of GO–TiO_2-400 were investigated. Fig. 10 illustrates that the photocatalytic efficiency of GO–TiO_2-400 in the degradation of 2E1H decreased as the relative humidity increased. The average photocatalytic efficiency for the degradation of 2E1H was 89% at a relative humidity of 20%, whereas it was 75% at a relative humidity of 80%. Jo and Kang [29] observed that the photocatalytic efficiency of gas-phase benzene, using UV-activated, polymer-supported TiO_2 fibers, decreased from 90% to 54% as the relative humidity increased from 20% to 90%. The decrease in the photocatalytic efficiencies at high relative humidity is ascribed to competition between contaminants and water molecules for adsorption sites on the photocatalyst surface.

Fig. 11 shows that the photocatalytic efficiency of GO–TiO_2-400 in the degradation of 2E1H decreased gradually from 83% to 61%, as the initial concentration increased from 0.1 to 1.5 ppm. Jo and Kang [29] showed that the photocatalytic efficiency in the degradation of benzene decreased from 85% to 9% as the initial concentration increased from 0.1 to 1.0 ppm. For low 2E1H initial concentrations, large numbers of the adsorption sites on the catalysts surface are available for adsorption of 2E1H molecules, elevating its photocatalytic efficiency. Meanwhile, the photocatalytic efficiency of GO–TiO_2-400 increased as the photocatalyst mass increased from 0.05 to 0.2 mg cm^{-2} (Fig. 12), probably because of the greater numbers of adsorption and photocatalytic reaction sites and larger amount of photon absorbance at high photocatalyst masses [30,31].

The reaction rate (r_R) was obtained via the following relationship:

$$r_R = \frac{f_u(C_{us} - C_{ds})Q_a}{A_p} \quad (4)$$

where C_{us} and C_{ds} are the upstream and downstream 2E1H concentrations (ppm), respectively; Q_a is the flow rate ($m^3\ s^{-1}$); A_p is the

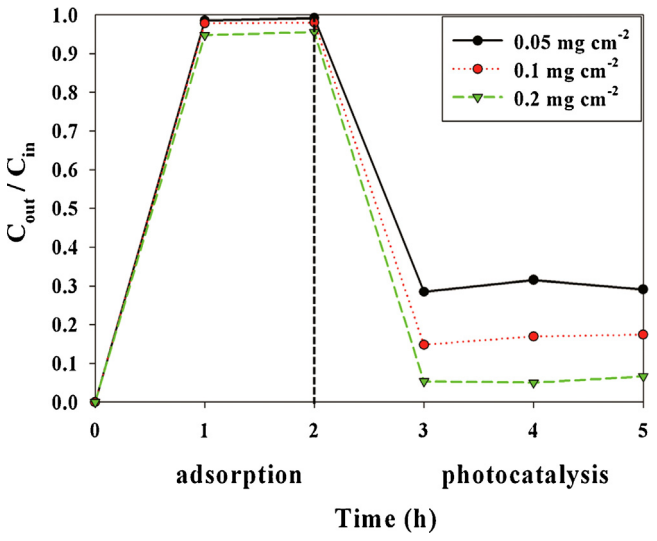

Fig. 12. Time-series ratios of input to output concentrations of 2E1H over GO–TiO_2-400 under visible-light irradiation, according to coated photocatalyst amount (0.05, 0.1, and 0.2 mg cm^{-2}).

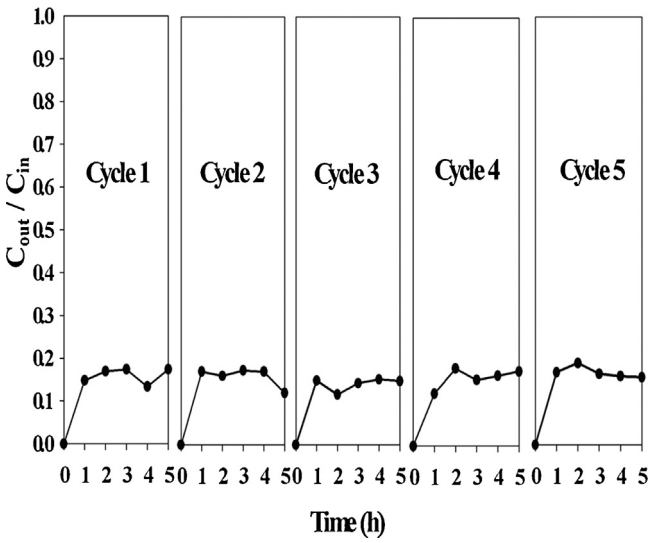

Fig. 13. Time-series ratios of input to output concentrations of 2E1H over GO–TiO_2-400 under visible-light irradiation, according to number of cycles (1–5 cycles); coated photocatalyst amount, 0.1 mg cm^{-2}.

sample surface area (m^2); and f_u is the unit-adjustment constant (40.9 μ-mol m^{-3} ppm^{-1}). Contrary to the photocatalytic efficiencies, the photocatalytic degradation rates of 2E1H increased as the initial concentration increased. The reaction rates for 0.1, 0.5, 1.0, and 1.5 ppm of 2E1H were 1.2×10^{-2}, 1.6×10^{-2}, 3.5×10^{-2}, and 5.3×10^{-2} μ-mol m^{-2} s^{-1}, respectively. Similarly, Jo and Kang [29] showed that, contrary to the photocatalytic efficiency, the reaction rate of *o*-xylene increased gradually as the initial concentration increased from 0.1 to 1.0 ppm. The higher photocatalytic efficiency with a lower reaction rate for a low initial concentration can be explained by greater adsorption competition at a low initial concentration, outweighing the reaction rate effect on the 2E1H photocatalytic degradation efficiency.

Experiment V was performed to examine the stability of GO–TiO_2-400 over five cycles of 2E1H decomposition. After each cycle, the catalyst was purified by allowing humidified air to flow over it for 10 h under light illumination. As shown in Fig 13, there was no appreciable loss of photocatalytic efficiency of GO–TiO_2-400 after five cycles, indicating that it had high stability.

3.3. Mineralization efficiency and intermediates

In Experiment IV, the mineralization and photocatalytic degradation efficiencies for gas-phase 2E1H over GO–TiO_2-400, which displayed the highest photocatalytic activity among the tested GO–TiO_2 hybrids, were examined at a relative humidity of 50%, photocatalyst coating amount of 0.1 mg cm^{-2}, flow rate of 1 L min^{-1}, and 2E1H input concentration of 0.8 ppm. The mineralization efficiency (E_M) was calculated using the CO_2 concentrations measured at the output air stream of the photocatalytic reactor:

$$E_M = \frac{[CO_2]_{out} \times 10^2}{(8 \times [2E1H]_{in} \times R_p)} \quad (5)$$

where $[CO_2]_{out}$ represents the CO_2 concentration (ppm) measured in the output air stream of the photocatalytic reactor. A multiplying factor (10^2) was used for percentage calculations, and the constant (8) denotes the number of carbon atoms in 2E1H (1 mol of 2E1H produces 8 mol of CO_2). $[2E1H]_{in}$ represents the 2E1H concentration (0.8 ppm) measured in the input air stream of the reactor and R_P denotes the photocatalytic degradation rate. The data in Table 3 reveals that the 2E1H mineralization efficiency (average value 55.1%) over GO–TiO_2-400 was lower than the photocatalytic degradation efficiency (average value 99.3%). These results are consistent with those reported for previous studies [32,33], in which other photocatalytic systems such as a TiO_2/UV lamp and multi-walled carbon nanotubes–TiO_2 nanofibers/daylight fluorescent lamp were used. Specifically, Jo and Kang [33] reported that the mineralization efficiency for a sub-ppm limonene concentration (1.6 ppm), determined using the multi-walled carbon nanotubes–TiO_2 nanofibers/daylight fluorescent lamp system, ranged from 8.3% to 91.1%, whereas the decomposition efficiency ranged from 90.1% to 99.9%, depending on the air residence time (7.8–78.0 s). Similarly, Sleiman et al. [32] reported a toluene mineralization efficiency (55–95%) that was lower than the photocatalytic degradation efficiency (90–100%) under UV illumination over TiO_2 deposited on a fibrous sheet. The lower 2E1H mineralization efficiency compared with the cor-

Table 3
Time-series and average CO and CO_2 concentrations, mineralization efficiencies, photocatalytic degradation ratios, and photocatalytic degradation efficiencies of photocatalytic degradation of 2E1H over GO–TiO_2-400.[a]

Time(h)	CO conc.(ppm)	CO_2 conc.(ppm)	Mineralization efficiency (%)	Photocatalytic ratio	Photocatalytic efficiency (%)
1	0.53	3.4	53.2	0.998	99.8
2	0.54	3.5	55.1	0.997	99.7
3	0.49	3.2	50.8	0.984	98.4
4	0.47	3.6	56.5	0.995	99.5
6	0.43	3.7	58.5	0.988	98.8
8	0.48	3.6	56.5	0.995	99.5
Average	0.49	3.5	55.1	0.993	99.3

[a] Number in parenthesis represents standard deviation; photocatalytic degradation ratio was calculated by dividing 2E1H output concentration by 2E1H input concentrations; photocatalytic efficiency was calculated by multiplying photocatalytic degradation ratio by 100.

Table 4
Concentrations of gas-phase intermediates produced during photocatalytic degradation of 2E1H over GO–TiO_2-400.[a]

Compound	Concentration (ppm)
3-Heptanone ($C_7H_{14}O$)	0.11
2-Ethyl hexanal ($C_8H_{16}O$)	0.21

[a] NA: not available.

responding photocatalytic degradation efficiency indicates that incompletely oxidized intermediates were generated during photocatalysis of 2E1H over the GO–TiO_2 hybrids.

Table 4 shows the gas-phase organic intermediates generated during photocatalysis of 2E1H over GO–TiO_2-400. Two gaseous organic compounds (3-heptanone, 0.11 ppm and 2-ethyl hexanal, 0.21 ppm) were the primary intermediates generated during the photocatalysis of 2E1H. 3-Heptanone and 2-ethyl hexanal accounted for approximately 13.8% and 26.3%, respectively, of the initial pollutant concentration (2E1H, 0.8 ppm). However, no intermediates adsorbed on the photocatalyst surface were detected using solid–liquid extraction, possibly because the amounts were below the analytical measurement limits. Unlike 2E1H, other VOCs have been widely investigated in terms of gaseous intermediate generation, using various photocatalytic systems. Debono et al. [34] identified benzaldehyde and cresols as major reaction intermediates and 12 minor VOCs or semi-VOCs during the photocatalytic degradation of gas-phase toluene (0.05–0.8 ppm) over P25 TiO_2 in a batch Pyrex chamber (120 L) under UV exposure. Sleiman et al. [32] reported generation of the same major reaction intermediates and six different minor VOCs or semi-VOCs during the photocatalytic degradation of toluene (0.02–0.4 ppm) at a relative humidity of 40% over UV-irradiated fibrous anatase TiO_2 in an annular flow-through reactor (0.085 L). They also observed several intermediates adsorbed on the TiO_2 surfaces; the intermediates were identified using a solvent mixture of methanol/water/NaOH and ion chromatography (IC), high-performance IC, and GC/MS analyses. Vildozo et al. [35] observed several gas-phase and adsorbed intermediates during the photocatalysis of a 2-propanol/toluene binary mixture over fibrous anatase TiO_2 under UV exposure in a continuous-flow reactor (0.050 L). In addition, the CO concentration generated during the photocatalysis of 2E1H over GO–TiO_2-400 varied between 0.43 and 0.54 ppm, with an average value of 0.49 ppm (Table 3). However, the CO concentrations were well below the 8-h average permissible exposure limit of 25 ppm [36], indicating that the generated CO was not a significant health hazard.

A plausible reaction mechanism for the photocatalytic reaction of 2E1H over GO–TiO_2 hybrids under visible light illumination is proposed in this study. When the GO–TiO_2 hybrids are exposed to visible light, an electron can directly be excited from GO to the conduction band of TiO_2, well-separating the charge carriers [19,25,36]. Therefore, the transferred electron in TiO_2 and the positive hole left on the GO surface would react with an oxygen molecule and a hydroxyl ion, respectively, to generate a superoxide ion and an hydroxyl radical, respectively. The superoxide ion and hydroxyl radical could then oxidize 2E1H molecules, which were previously adsorbed on GO surface and then migrated to TiO_2 surface, to produce CO_2, CO, 3-heptanone, 2-ethyl hexanal, and unidentified intermediates.

4. Conclusions

In the present study, we investigated whether high-temperature (>300 °C) post-treatment of GO–TiO_2 hybrids can enhance their photocatalytic performances without significant loss of their hybrid natures. To this end, GO–TiO_2 hybrids were synthesized using a chemical mixing method, followed by post-treatment under various thermal conditions. The adsorption properties and photocatalytic performances of the synthesized GO–TiO_2 hybrids and neat TiO_2 were examined in the degradation of gaseous 2E1H in continuous-flow mode. The morphological and optical characteristics of the GO–TiO_2 hybrids showed that the TiO_2 nanoparticles were successfully embedded into the GO sheets, and that they displayed photocatalytic activities under visible-light illumination. The photocatalytic activities of the thermal post-treated GO–TiO_2 hybrids were superior to those of the untreated GO–TiO_2 hybrid and neat TiO_2 samples. The thermal post-treatment temperature crucially affected both the adsorption properties and photocatalytic performances of the GO–TiO_2 hybrids. The thermal treatment temperature could be increased up to at least 400 °C without significant damage to the photocatalytic performances of the GO–TiO_2 hybrids. Three process parameters (relative humidity, initial contaminant concentration, and catalyst mass) were found to be important for the photocatalytic activities of the GO–TiO_2 hybrids. A cycling test showed the stability of the GO–TiO_2 hybrids. In addition, the 2E1H mineralization efficiency was lower than the photocatalytic efficiency, indicating the formation of incompletely oxidized products. Two gas-phase organic intermediates were observed, but adsorbed intermediates could not be detected. This study also found that toxic CO gas was generated during the photocatalysis of 2E1H; however, its concentration was insufficient to cause adverse health effects.

Acknowledgement

This work was supported by the National Research Foundation of Korea (NRF) grant funded by the Korean government (MEST) No. 2011-0027916 and GCRC-SOP No. 2011-0030013. We thank Hyun-Jung Kang (research associate), Joon Yeob Lee (Ph.D student) and Yu-Rim Shin (Master student) in the Department of Environmental Engineering, Kyungpook National University, for conducting sample collection and analyses. We also appreciate the referee for their valuable suggestions.

References

[1] I. Annesi-Maesano, N. Baiz, S. Banerjee, P. Rudnai, S. Rive, SINPHONIE Group, J. Toxicol. Environ. Health B Crit. Rev. 16 (2013) 491–550.
[2] IARC (International Agency for Research on Cancer). List of classifications by alphabetical order. Accessed at November 23 (2014). Available at: http://monographs.iarc.fr/ENG/Classification/index.php
[3] M. de Blas, M. Navazo, L. Alonso, N. Durana, M.C. Gomez, J. Iza, Sci. Total Environ. 426 (2012) 327–335.
[4] S.H. Shin, W.K. Jo, Environ. Sci. Pollut. Res. 20 (2013) 3696–3707.
[5] P. Wolkoff, Int. J. Hyg. Environ. Health 216 (2013) 371–394.
[6] M.S. Zuraimi, C.-A. Roulet, K.W. Tham, S.C. Sekhar, K.W. David Cheong, N.H. Wong, K.H. Lee, Build. Environment. 41 (2006) 316–329.
[7] L. Ernstgård, D. Norbäck, T. Nordquist, G. Wieslander, R. Wålinder, G. Johanson, Indoor Air 20 (2010) 168–175.
[8] S. Chino, S. Kato, J. Seo, J. Kim, J. Adhesion Sci. Technol. 27 (2013) 659–670.
[9] T. Cecchi, Build. Environ. 82 (2014) 655–665.
[10] T. Ochiai, A. Fujishima, J. Photochem. Photobiol. C 13 (2012) 247–262.
[11] A.D. Paola, E. García-López, G. Marcì, L. Palmisano, J. Hazard. Mater. 211–212 (2012) 3–29.
[12] M.A. Henderson, Surf. Sci. Rep. 66 (2011) 185–297.
[13] R.M. Mohamed, D.L. McKinney, W.M. Sigmund, Mater. Sci. Eng. R 73 (2012) 1–13.
[14] I.V. Lightcap, T.H. Kosel, P.V. Kamat, Nano Lett. 10 (2010) 577–583.
[15] R. Leary, A. Westwood, Carbon 49 (2011) 741–772.
[16] G. Jiang, Z. Lin, C. Chen, L. Zhu, Q. Chang, N. Wang, W. Wei, H. Tang, Carbon 49 (2011) 2693–2701.
[17] W.K. Jo, H.J. Kang, Powder Technol. 250 (2013) 115–121.
[18] T.N. Lambert, C.A. Chavez, B. Hernandez-Sanchez, P. Lu, N.S. Bell, A. Ambrosini, T. Friedman, T.J. Boyle, D.R. Wheeler, D.L. Huber, J. Phys. Chem. C 113 (2009) 19812–19823.
[19] T.-D. Nguyen-Phan, V.H. Pham, E.W. Shin, H.-D. Pham, S. Kim, J.S. Chung, E.J. Kim, S.H. Hur, Chem. Eng. J. 170 (2011) 226–232.
[20] M. Roso, A. Lorenzetti, C. Boaretti, D. Hrelja, M. Modesti, Appl. Catal. B 176 (2015) 225–232.

[21] W. Hummers, R. Offeman, J. Am. Chem. Soc. 80 (1958) 1339.
[22] M.L. Chen, C.Y. Park, J.G. Choi, W.C. Oh, J. Kor. Ceramic Soc. 48 (2011) 147–151.
[23] N. Pan, D. Guan, Y. Yang, Z. Huang, R. Wang, Y. Jin, C. Xia, Chem. Eng. J. 236 (2014) 471–479.
[24] Z. Lei, L. Lu, X.S. Zhao, Energy Environ. Sci. 5 (2012) 6391–6399.
[25] L.M. Pastrana-Martínez, S. Morales-Torres, V. Likodimos, J.L. Figueiredo, J.L. Faria, P. Falaras, A.M.T. Silva, Appl. Catal. B 123–124 (2012) 241–256.
[26] B. Tryba, M. Toyoda, A.W. Morawski, M. Inagaki, Appl. Catal. B 71 (2007) 163–168.
[27] Y. Zhang, Z.-R. Tang, X. Fu, Y.-J. Xu, ACS Nano 4 (2010) 7303–7314.
[28] A. Du, Y.H. Ng, N.J. Bell, Z. Zhu, R. Amal, S.C. Smith, J. Phys. Chem. Lett. 2 (2011) 894–899.
[29] W.K. Jo, H.J. Kang, Ind. Eng. Chem. Res. 52 (2013) 4475–4483.
[30] Q.L. Yu, H.J.H. Brouwers, Appl. Catal. B 92 (2009) 454–461.
[31] A. Turolla, A. Piazzoli, J.F. Budarz, M.R. Wiesner, M. Antonelli, Chem. Eng. J. 271 (2015) 260–268.
[32] M. Sleiman, P. Conchon, C. Ferronato, J.-M. Chovelon, Appl. Catal. B 86 (2009) 159–165.
[33] W.K. Jo, H.J. Kang, J. Hazard. Mater. 283 (2015) 680–688.
[34] O. Debono, F. Thevenet, P. Gravejat, V. Hequet, C. Raillard, L. Lecoq, N. Locoge, Appl. Catal. B 106 (2011) 600–608.
[35] D. Vildozo, R. Portela, C. Ferronato, J.-M. Chovelon, Appl. Catal. B 107 (2011) 347–354.
[36] USEPA (United States of Environmental Protection Agency), An Introduction to Indoor Air Quality (IAQ): Carbon Monoxide (CO) (2014). Available online at http://epa.gov/iaq/co.htmlhttp://epa.gov/iaq/co.html